

# Surfactants assisted solvothermal derived titania nanoparticles: synthesis and simulation

Davoud Dastan<sup>1</sup> · Nandu Chaure<sup>1</sup> · Moses Kartha<sup>1</sup>

Received: 24 November 2016 / Accepted: 25 January 2017 / Published online: 7 February 2017  
© Springer Science+Business Media New York 2017

**Abstract** Solvothermal method was used to prepare titanium dioxide (TiO<sub>2</sub>) nanoparticles (NP's) of various morphologies at 180 °C growth temperature. Acetic acid and oley amine were used as surfactants. The powder of TiO<sub>2</sub> was annealed at 550 and 950 °C for 18 and 24 h. The influence of surfactants on the morphology of titania NP's was investigated using transmission electron microscopy (TEM). The structural, optical, and molecular properties of titania NP's are investigated by means of X-ray diffraction, UV–visible, Photoluminescence, and Fourier Transform Infrared. The physical properties, surface area and pore volume, of the samples were investigated by Brunauer-Emmett-Teller and Barrett-Joyner-Halenda measurement. The results illustrated type IV adsorption isotherms for all samples, implying the characteristics of mesoporous materials (2–50 nm). Furthermore, the hysteresis loops shifted to higher relative pressure, indicating that the specific surface area increases and the pore size decreases after heat treatment. Micrograph images acquired from TEM portrayed different shapes such as irregular spherical, rounded rectangular, truncated rhombic, and rod-like for titania NP's when various surfactants were used. Monte-Carlo simulation carried out for pristine and rutile titania NP's as representative samples explained the growth mechanism of titania NP's and corroborated the formation of spherical and rod-like structures due to attractive and repulsive interactions among particle respectively.

## 1 Introduction

Semiconductor oxides have been vastly investigated during last decades. Titania has outstanding optical, chemical, and physical features for different applications [1–5]. It possesses large band gap and high dielectric constant (high- $k$ ) [2, 6–12] and can be used as a gate dielectric for field effect transistors (FET's). Titania has variety of applications such as sensors, solar cells, optical and photochromic devices, planar wave guides, and light scattering [11, 13–16]. The change in the shape of TiO<sub>2</sub> has been affected by factors such as chemical composite, calcination temperature, phase transmutation, precursors, and the chemical reactions.

Titanium *n*-butoxide and several growth temperature were used as a precursor for the preparation of titania NP's [4], but in this study, the single growth temperature, constant surfactant concentrations, and titanium isopropoxide (TIP, as a precursor) were employed for the preparation of TiO<sub>2</sub> NP's subjected to post-heat treatment. TiCl<sub>4</sub> is another forerunner which has been employed for the preparation of titania NP's, but it has the drawback of using under inert gas such as argon, because it has the problem of sensitivity to humidity.

Solvothermal technique is employed for the synthesis of titania NP's as it is a non-toxic method for the preparation of the pure and homogeneous nanoparticles [5, 6]. Additionally, it is relatively a low cost and easy processing method. The present article aims to investigate the influence of using various surfactants on the properties of titania NP's, particularly morphological features and then investigate the other characteristics such as physical, molecular, structural, and optical properties at 180 °C reaction temperature for pristine and post-annealed samples, because the applications of titania NP's are size and shape dependant. The changes in morphology of TiO<sub>2</sub> NP's were

✉ Davoud Dastan  
d.dastan61@yahoo.com

<sup>1</sup> Department of Physics, Savitribai Phule Pune University, Pune, Maharashtra 411007, India

further corroborated by Monte-Carlo (MC) simulation. To the authors best knowledge, the shape of titania NP's were experimentally investigated, but in this research work, both experimental and theoretical studies were differently used to investigate the various shapes of TiO<sub>2</sub> NP's.

## 2 Materials and methods

### 2.1 Materials

Titanium isopropoxide (TIP, C<sub>12</sub>H<sub>28</sub>O<sub>4</sub>Ti), Acetic Acid, C<sub>2</sub>H<sub>4</sub>O<sub>2</sub>, Oley amine, C<sub>18</sub>H<sub>37</sub>N, Absolute ethanol, C<sub>2</sub>H<sub>5</sub>OH, and Acetone, C<sub>3</sub>H<sub>6</sub>O were used for the preparation of titania NP's. These materials were purchased from Sigma–Aldrich and used without further purification.

### 2.2 Synthesis

Solvothermal method was employed to prepare titanium dioxide NP's. Titanium isopropoxide (TIP), as a source of titania, was incrementally added to a mixture of acetic acid (AA) and absolute ethanol and the solution was under strong stirring for 1 hour at room temperature. A molar ratio, 0.1:9:1, of AA/ethanol/TIP was used which was changed to 0.2:9:1 for OM/ethanol/TIP [3, 11]. The consequent suspension was transmuted into a Teflon-lined autoclave, sealed with a crust made of stainless steel, and reacted at 180 °C for 24 h to get the mono-dispersed titania powder which was cooled at ambient condition. Then, the solution was centrifuged at 12,000 rpm and washed with ethanol for three times. The resulted precipitate was dried at ambient condition and crushed in very small quantity. Finally, the dried powder of TiO<sub>2</sub> was calcinated at 550 and 950 °C for 18 and 24 h respectively [4–6, 11].

### 2.3 Characterization

Phase identification and optical studies of the pristine and annealed titania NP's were investigated using X-Ray Diffraction (XRD, D8, Advanced Bruker Diffractometer), UV Visible (Jasco UV/Vis spectrophotometer), and Photoluminescence (Fluorolog HORIBA JOBINYVON). The molecular and morphological properties of the specimens were studied using Fourier Transform Infrared (Jasco FTIR spectrometer) and Transmission Electron Microscopic (TEM, TECHNAI G<sup>2</sup> 20U-Twin (FEI, Netherlands) DST-FIST). The physical properties of the samples were investigated using Brunauer-Emmett-Teller (BET) surface area analysis and Barrett-Joyner-Halenda (BJH) pore size and volume analysis (Surface Area Analyzer, Quantachrome Instrument, autosorb iQ<sub>2</sub>, automated gas sorption analyzer).

Monte Carlo simulation was used to investigate the growth mechanism of titania NP's.

## 3 Results and discussion

### 3.1 Structural properties: X-ray diffraction

XRD analysis was used to study the structural properties of titania NP's. Figure 1A–C, depicts the representative XRD patterns of pristine and annealed at 550 and 950 °C TiO<sub>2</sub> NP's. The representative XRD spectra's of pristine titania NP's using a mixture of AA and OM is presented in the Fig. 1A. Figure 1B, C is related to the XRD patterns of samples calcinated at 550 and 950 °C respectively. XRD pattern of the as-prepared titania NP's portrayed the peaks at nearly 25.27°, 37.81°, 48.11°, 53.93°, 55.12°, 62.68°,

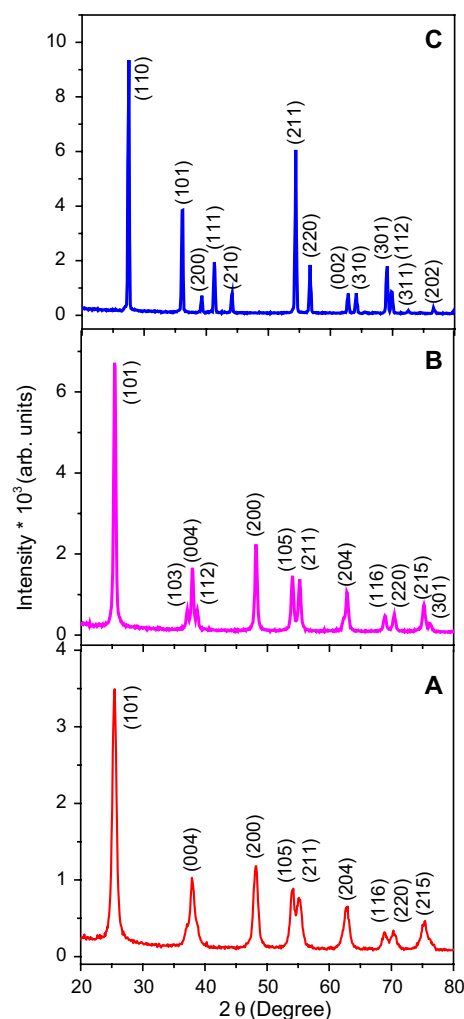


**Fig. 1** Representative XRD patterns recorded for **A** pristine, calcinated at **B** 550 °C, and **C** 950 °C TiO<sub>2</sub> NP's in presence of AA + OM as surfactants

68.84°, 70.34°, and 75.20°, ascribed to (101), (004), (200), (105), (211), (204), (116), (220), and (215) Miller planes respectively, which are attributed to the crystalline structure of the pure anatase phase of TiO<sub>2</sub>. Similarly, the nanoparticulates of TiO<sub>2</sub> annealed at 550 °C demonstrated the pure anatase phase which was corroborated with all the observed Miller planes for pristine sample along with three additional planes (103), (112), and (301) at 2θ of around 37.00°, 38.60°, and 76.10° [11, 17–29].

However, the formation of pure rutile phase of titania NP's is illustrated after annealing at 950 °C through the Miller indexes (110), (101), (200), (111), (210), (211), (220), (002), (310), (301), (112), (311), and (202) associated with the peaks positioned at approximately 2θ = 27.36, 36.02, 39.10, 41.19, 43.96, 54.22, 56.51, 62.68, 63.97, 68.95, 69.74, 72.33, and 76.41 [17, 19, 30, 31]. As can be clearly seen, the peaks appeared in the XRD patterns of the pristine and annealed at 550 °C titania NP's are predominantly not totally the same, with three extra peaks and crystallinity enhancement for annealed sample, indicating the pure anatase phase, while the phase has been completely transmuted to pure rutile at 950 °C.

In contrast to our previous study in which sol–gel provided amorphous phase for pristine titania NP's [3, 7, 11], solvothermal method employed in this study, disclosed a pure anatase phase for as-prepared specimen and illustrated a remarkable improvement in the crystallinity of both pristine and calcinated TiO<sub>2</sub> NP's. Previous studies, [4] reported only anatase phase of titania for several reaction temperatures, and [32] investigated anatase phase for annealed at 800 and 900 °C titania-silica composites and a mixture of all three phases of TiO<sub>2</sub> for the same composite at 1000 °C annealing temperature while in this study, the development of pure anatase and pure rutile phase were observed for pristine, calcinated at 550 °C [3, 7, 11], and 950 °C titania NP's respectively, at growth temperature 180 °C [3, 7].

The presence of pure anatase phase for as-prepared sample suggesting that the solvothermal method is a low cost technique for the preparation of anatase titania NP's, because the anatase phase which normally appears in the temperature range 350–700 °C, is now produced without any post heat treatment, and this is substantially important for many useful applications such as solar cells and batteries. The crystallite size of pristine and annealed titania NP's are evaluated using Scherrer formula [3, 7, 21, 24]:

$$D = K\lambda/\text{Cos} \quad (1)$$

where, D is the crystallite size (nm), β is the full width at half-maximum height (FWHM), and θ is the Bragg diffraction angle (°), λ is the wavelength of the X-ray radiation (Cu Kα = 0.15 nm), and K is the Scherrer constant (0.89). It is well known that the size of particle depends on

calcinations temperature that increases when the annealing temperature increases. Hence, calcinated samples at 950 °C exhibited higher crystallite size than those of annealed at 550 °C and the as-prepared specimens. This phenomenon is most likely owing to the aggregation and recrystallization of TiO<sub>2</sub> NP's after heat treatment [3, 7, 11].

## 3.2 Optical properties

### 3.2.1 Absorption and transmittance spectra

The optical properties of pristine and annealed at 550 and 950 °C titania NP's have been investigated using UV–vis and photoluminescence (PL) spectroscopy at room temperature. The representative of absorption and transmission spectra of as-prepared and annealed at 550 and 950 °C titania NP's are delineated in Fig. 2. The absorption edge, extrapolating the onset line towards X-axis, was almost 393 nm for pristine titania NP's (Fig. 2A) which was red shifted to 396 and 423 nm, after heat treatment at 550 (Fig. 2B) and 950 °C (Fig. 2C) respectively. It is therefore expected that, the energy band gap (E<sub>g</sub>), calculated using expression 2, reduces upon heat treatment.

$$E_g = 1239/\lambda \quad (2)$$

where λ is the wavelength of the optical absorption edge. The transmittance spectra of pristine and calcinated titania

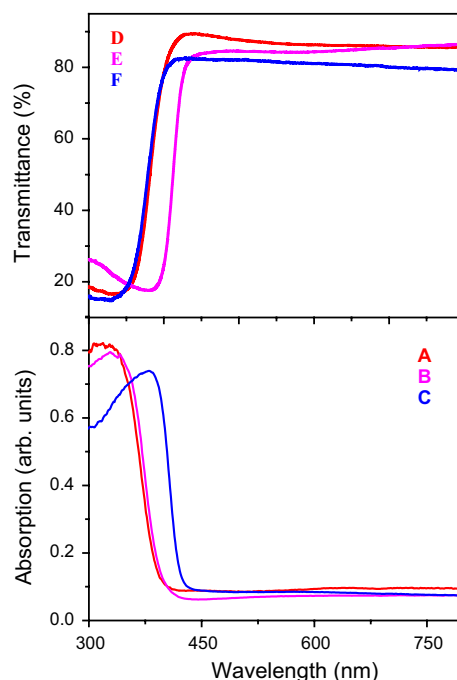


**Fig. 2** Representative absorption and transmittance spectra of A, D pristine, calcinated at B, E 550 °C, and C, F 950 °C TiO<sub>2</sub> NP' in existence of AA + OM as surfactants

NP's is depicted in the Fig. 2D–F. It is expected that the energy band gap and transmittance reduce after calcination. The decrease in the energy band gap is possibly owing to the aggregation of nanoparticles or transmutation of titania phase from anatase to rutile while the reduction in the transmittance is owing to the increase in surface scattering which is attributed to the surface roughness. The reduction in band gap is of interest for the application of titania in photocatalytic devices [3, 11, 33–37].

### 3.2.2 Photoluminescence spectra

The study of the efficacy of charge carrier trapping, immigration and transfer of the charge carriers and recombination of electron–hole pairs, either instantly (band to band) or indirectly (via a bandgap state), was performed using photoluminescence spectra (PL). Figure 3 portrays the representative PL spectra of pristine and annealed at 550 and 950 °C titania NP's in presence of AA and OM as

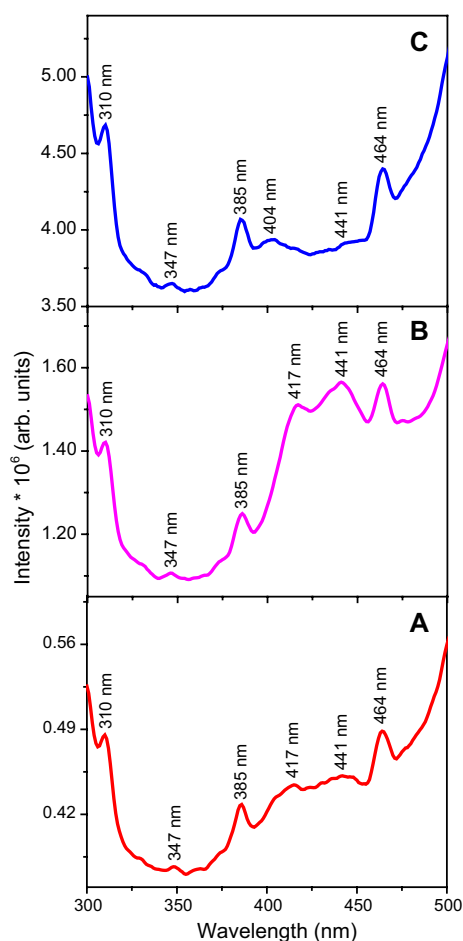


**Fig. 3** Representative photoluminescence spectra of **A** pristine, calcinated at **B** 550 °C, and **C** 950 °C TiO<sub>2</sub> NP's in existence of AA + OM as surfactants, and at the excitation wavelength 280 nm

surfactants at ambient condition with excitation wavelength 280 nm. As it can be conspicuously seen, the intense luminescence peaks are located in the visible region. The positions of peaks are approximately the same except the luminescence peak located in the near band gap emission around 404 nm which is attributed to the band gap of rutile crystal structure of titania NP's (Fig. 3C). This peak is appeared only for sample annealed at 950 °C and not emerged for as-prepared and annealed at 550 °C samples.

Moreover, the PL intensity is noticeably increased which veritably implying to an augmentation in the higher recombination rate of excited electrons and holes after heat treatment. On other aspect, this is owing to the fact that calcination can cause superficial traps and defect levels between the valance and conduction bands, which in turn can create the sub-bands in the proximity of emanated main peaks owing to the variation in the morphology and crystallite size. As a consequence of calcination, the number of hydroxyl group at the valance band of titania and superoxide radical anion (O<sup>2-</sup>) reduces. Consequently, it leads to high intensity and high rate of charge carrier recombination, which in turn considerably reduces and the photocatalysis activity.

Two main emission peaks located at nearly 385 and 464 nm are respectively attributed to the band gap transition of anatase phase of nanoparticulates titania and the charge-transfer transition from Ti<sup>3+</sup> to oxygen anion in a TiO<sub>6</sub><sup>8-</sup> complex as well as oxygen vacancies at the surface [3, 7, 33–38]. The spectra exhibited a small hump at approximately 417 nm that matches with anatase phase of TiO<sub>2</sub> (Fig. 3A, B). The luminescence peak at 310 nm and two tubercles at nearly 347 and 441 nm emerged for all samples which could be originated from the localized surface states (defects) such as Ti<sup>4+</sup>-OH owing to recombination of electron–hole pairs [7, 33, 34, 38].

### 3.3 Molecular study

The molecular studies of the pristine and thermally treated at 550 and 950 °C TiO<sub>2</sub> NP's were acquired by means of Fourier transform infrared (FTIR) spectroscopy. Figure 4A–C depicts the representative FTIR of the pristine and samples calcinated at 550 and 950 °C in the existence of a mixture of AA and OM as surfactants. FTIR measurements preformed over an effective range of 700 to 4000 cm<sup>-1</sup> at 100 reaction cycles at room temperature. IR spectrum of as-prepared TiO<sub>2</sub> showed asymmetrical stretching vibration between 3400 and 3500 cm<sup>-1</sup> which is attributed to the stretching vibration mode of O–H band.

The intensity of this band decreases as the calcinations temperature increases. This could be due to the fact that water in the specimen is physically adsorbed in air. As it can be seen, the FTIR spectra of this unsymmetrical

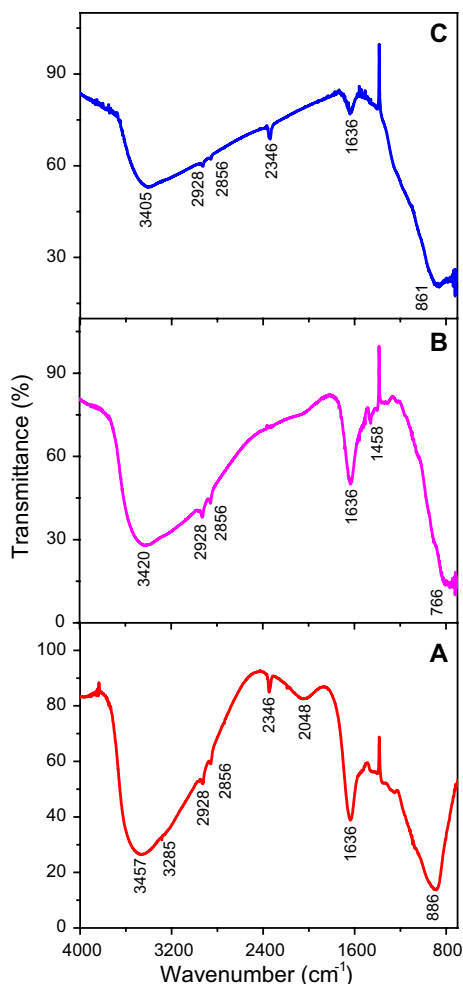


**Fig. 4** Representative Fourier Transform Infrared (FTIR's) spectroscopy of TiO<sub>2</sub> NP's (A) as-prepared, B and C samples annealed at 550 and 950 °C using a mixture of AA + OM as surfactants

broad band is transferred towards lower frequency range after annealing which betokens the possible involvement of the functional groups on the surface of titania NP's [34, 39–47]. The small band emerged at 3200 cm<sup>-1</sup> is owing to the symmetrical vibrations of primary amides (NH<sub>2</sub>) [25, 26, 42, 43].

The other peaks in the FTIR spectra are due to entity of organic molecules on the surface of TiO<sub>2</sub> NP's. The stretching vibrations bands at 2928 (asymmetric) and 2856 (symmetric) cm<sup>-1</sup> were assigned to the bending vibration of alkyl (methylene or -CH<sub>2</sub> and methyl or -CH<sub>3</sub> respectively) groups. The asymmetric mode causes a larger dipole moment to rise and has greater intensity than the symmetric mode [42, 43, 45, 46]. The set of FTIR transmittance spectra in the interval of 700–900 cm<sup>-1</sup> are assigned to the lattice vibrations of titanium dioxide. This matches well with the reported value for titanium dioxide NP's [46, 47].

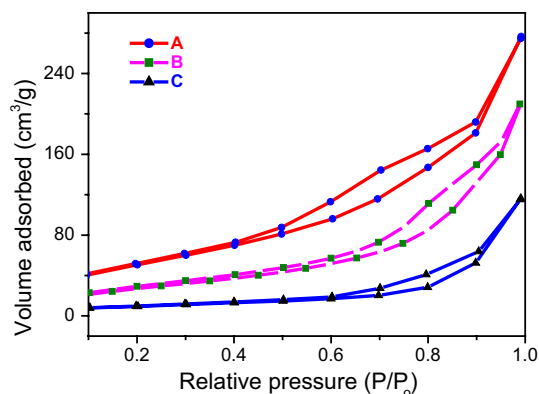


**Fig. 5** Representative physical and structural properties of (A) as-prepared, samples annealed at B 550 and C 950 °C mesoporous titania NP's using AA + OM as surfactants

The C=N and C=C bands normally appear in the region of the infrared spectrum 1850–1620 cm<sup>-1</sup>. However, the C=N band gives rise to a strong absorption while the C=C band is a weak absorber. Hence, the respective IR peak at 1636 cm<sup>-1</sup> can be assigned to asymmetric band stretching C=N group whose intensity decreases at 950 °C [26, 40, 42, 44] and the medium absorption with a minima at 1458 cm<sup>-1</sup> can be attributed to the bending vibrations of C=C [41, 42]. The intense narrow band at 2346 cm<sup>-1</sup> is identified in the FTIR spectra which is absent in the pattern of calcinated specimens, is related to the bending vibrations of C=O group or corresponds to ketone carbonyl group. A C≡C band at almost 2048 cm<sup>-1</sup> is a weak stretch for alkynes group [42]. The above peaks disclosed the formation of nanoparticulates of TiO<sub>2</sub>.

### 3.4 Physical properties: Brunauer-Emmett-Teller (BET) surface area analysis and Barrett-Joyner-Halenda (BJH) pore size and volume analysis

Figure 5A–C is the representative nitrogen adsorption–desorption isotherms and pore size distribution curve of pristine and annealed titania NP's. The adsorption isotherm of pristine sample is depicted in Fig. 5A and the adsorption isotherms of the samples annealed at 550 and 950 °C are delineated in Fig. 5B, C. Titania NP's are thermally treated at high temperature in vacuum to remove the possible contaminants and BET isotherm of the samples is evaluated by physical adsorption of nitrogen at a temperature of 77.350 K. In fact, the amount of adsorbate gas molecules on the outer surface of titania NP's and the area of cross-section of nitrogen gas, 16.2 Å<sup>2</sup>, are useful for calculating the surface area of titania NP's. On the other hand, van der Waals forces between nitrogen molecules and titania surface area is useful for the calculating the BET isotherm.

The nitrogen adsorption–desorption of pristine and annealed samples demonstrated the type-IV isotherms (2–50 nm) and distinct hysteresis loops of type-H<sub>3</sub> according to IUPAC classification [18, 25, 26, 29]. The shift in the isotherms of samples towards higher relative pressure, implying that the specific surface area and pore volume decrease but pore diameter increases upon heat treatment which is due to increase in the crystallite size and the collapse of pore structure of TiO<sub>2</sub> NP's at higher annealing temperature [25, 26, 29]. The pore diameter of TiO<sub>2</sub> NP's was less than 11 nm whereas the surface area of the pristine, and samples annealed at 550 and 950 °C were 192.08, 103.63, 35.37 m<sup>2</sup>/g respectively.

Other investigations focused on the physical properties of mesoporous titania–silica [32], TiO<sub>2</sub>–Graphene Nanosheets (GNS), and 3D TiO<sub>2</sub>–GNS–Carbon nanotubes nanocomposites [18], and tungstophosphoric acid/mesoporous titania synthesized by urea-templated sol–gel annealed at different temperatures [26]. Similarly, nitrogen adsorption–desorption isotherms and the corresponding pore-size distribution of titania NP's, nanorods and titania spheres at different temperatures were investigated by Shalan et al. [29] and Jiang et al. [25] respectively.

NP's have been incorporated into many products and devices. They have a high surface-to-volume ratio which increases surface reactivity. The enhanced surface area and pore diameters are fruitful for applications such as heterogeneous catalysts and strong acids with high acidity. These properties are important for processing, blending of chemical products, stability, and toxicity of new materials [32]. The results of the physical properties of titania NP's are listed in the Table 1.

### 3.5 Morphology and microstructure analysis

#### 3.5.1 High resolution transmission electron microscopy

The morphology and features of the pristine and annealed at 950 °C titania NP's were further analyzed using transmission electron microscopy (TEM). Complementary to XRD, representative TEM micrographs and their corresponding electron diffraction patterns including selected area electron diffraction (SAED) and energy-dispersive X-ray spectroscopy (EDS) of TiO<sub>2</sub> NP's grown by a solvothermal

process were used to assess the morphology, the particle size, and phase identification of as-prepared and annealed samples.

In order to prepare the materials for TEM analysis, the powder samples were suspended in ethanol and sonicated with ultrasonic agitation for a long period of time so that the finely dispersed solution is achieved and individual particles are properly separated. Then, an aliquot of the suspension were dropped uniformly onto carbon mesh coated copper grids and dried in air. The micrographs were obtained using TEM at accelerating voltage 200 kV. The microscope is equipped with a Schottky-type field emission gun, an ultra high resolution configuration and in-column omega-type energy filter. HRTEM digital images were acquired using a CCD camera and digital micrograph software from GATAN.

The micrographs TEM images of the pristine and annealed at 950 °C titania NP's prepared using AA and a mixture of AA and OM as surfactants were recorded at room temperature. The TEM image of as-prepared sample prepared using AA consisted of a mixture of almost irregular spherical and rounded rectangular (Fig. 6A) whereas the formation of elongated spherical and truncated-rhombic shape were demonstrated for the sample prepared using OM as a surfactant and calcinated at 550 °C (Fig. 6B). Interestingly, the micrographs of rutile titania exhibited a rod-like structure with clear grain boundaries in presence of AA and OM as surfactants (Fig. 6C). The reason for this is consolidation of the individual particles, because the functional groups of carboxylic acid have been tightly bound onto the surface of titania to form a rod-like structures. Consequently, titania NP's, prepared using different surfactants, remarkably demonstrated the heterogeneous morphology [4, 19, 20, 47].

Acetic acid produces carboxyalkoxide groups that decelerate the hydrolytic condensation procedure but OM improves the enhancement of nonhydrolytic condensation through the reaction between aminolysis and titanium carboxylalkoxide. Therefore, the morphologies of TiO<sub>2</sub> NP's can be controlled using AA, OM, and a mixture of AA and OM as surfactants. Only spherical shape of titania NP's for a ratio 1:6:4 of titanium n-butoxide/oleic acid/OM was addressed at reaction temperature 180 °C by Cao-Thang et al. [4], while our investigations have shown various

**Table 1** Representative physical and structural properties of as-prepared and annealed at 550 and 950 °C mesoporous titania NP's using AA + OM as surfactants

Results Tempt. (°C)	Phase identification	Average Crystallite size (nm)	Surface area (m <sup>2</sup> /g)	Pore volume (cm <sup>3</sup> /g)	Pore diameter (nm)
Pristine	Pure Anatase	15	192.08	0.43	4.46
550	Pure Anatase	25	103.63	0.33	6.30
950	Pure Rutile	35	35.37	0.18	10.02

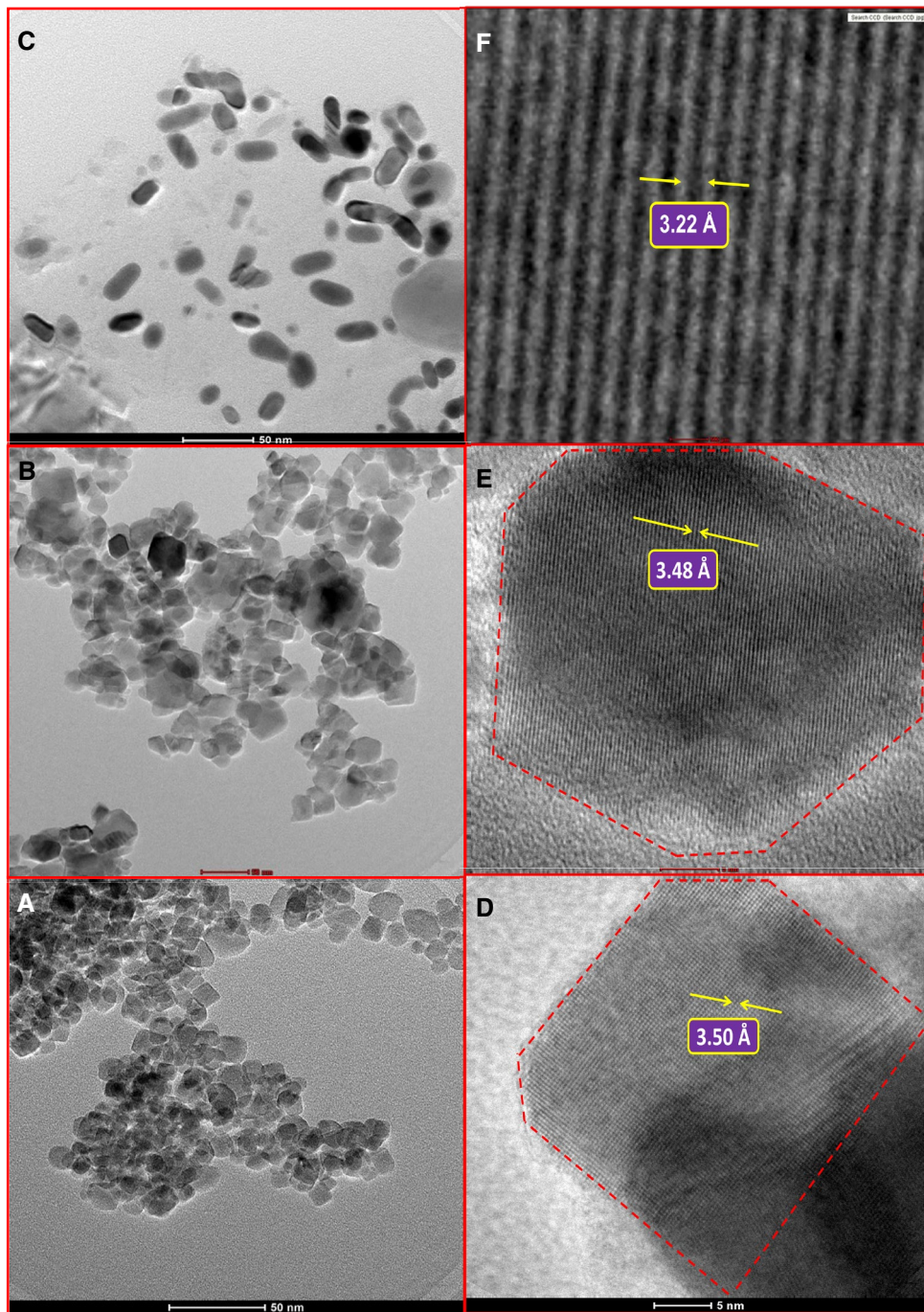


**Fig. 6** Transmission electron microscopy (TEM) image and high resolution transmission electron microscopy (HRTEM) of (A, D) as-prepared in presence of AA, B, E and C, F annealed at 550 and 950 °C titania NP's in presence of OM and AA + OM as surfactants, respectively

morphologies for the ratios, 1:9:0.1 and 1:9:0.1:0.2 of TIP/ethanol/AA and TIP/ethanol/AA/OM respectively, at the same growth temperature after post-annealing.

The size of particles was evaluated from the length of shorter and longer axis in TEM micrographs which was in the range of 5 to 35 nm. Figure 6A illustrates the TEM image of as-prepared TiO<sub>2</sub> NP's with an average particle

size of about 10 nm (5–15 nm). Figure 6B demonstrates that the particle size of sample annealed at 550 °C is almost 15 to 25 nm, while the average particle size for sample annealed at 950 °C is roughly 20–35 nm (Fig. 6C). Hence, the increase in the particle size is obvious upon heat treatment which is due to the change in the crystal structures after calcination. The titania NP's of smaller

size are of interest for applications such as photocatalysis activity and transparent optical coating [19, 23, 47].

The phases of as-prepared and annealed titania NP's were further analyzed by high resolution transmission electron microscopy (HRTEM). HRTEM of as-prepared (Fig. 6D) and sample heated at 550 °C (Fig. 6E) clearly indicate the presence of anatase phase of titania NP's with the interplanar spacing of 3.50 and 3.48 Å respectively, that are matched with the crystallographic plane (101) [8, 29, 48]. Figure 6F shows the HRTEM of the sample heated at 950 °C with a highly ordered lattice spacing of 3.22 Å corresponded with the (110) crystal plane [31].

### 3.5.2 Chemical analysis and selected area diffraction pattern

Selected area electron diffraction pattern (SAED) of titania NP's with clear lattice rings are depicted in Fig. 7A–C. There is a strong contrast between the dark edges and bright centers which implies that the prepared TiO<sub>2</sub> samples were highly crystalline. The lattice fringes (101), (004), (200), (105), (204), (116), and (215) corresponding to the d-spacing 3.50, 2.36, 1.86, 1.68, 1.64, 1.46, 1.35, and 1.26 Å respectively, show the SAED of as-prepared TiO<sub>2</sub> NP's (Fig. 7A) [20, 23, 48]. The crystalline lattice planes (101), (103), (004), (112), (200), (105), (211), and (204) are ascribed to the lattice d-spacing of 3.48, 2.40, 2.35, 2.31, 1.84, 1.67, 1.64, and 1.45 Å respectively (Fig. 7B). These results confirm the presence of pure anatase phase of titania NP's for as-prepared and sample annealed at 550 °C [21, 24]. Figure 7C delineates the transformation of anatase to rutile during solvothermal treatment. This diffraction spots consists of the slabs (110), (200), (111), (210), (211), (220), (301), and (112) corresponding to d-spacing 3.22, 2.20, 2.12, 2.02, 1.66, 1.60, 1.35, and 1.32 Å which are ascribed to the rutile phase of titanium dioxide NP's. Consequently, the SAED patterns corroborate the results of XRD [20, 48].

Energy dispersive X-ray spectroscopy (EDS) was used to identify the elements present in the prepared samples. The representative EDS of as-prepared and annealed samples are depicted in Fig. 7D–F. Titanium and oxygen with high weight percentages are present in all specimens as the main elements with the atomic ratio of Ti and O as 1:2. Additionally, the presence of small fraction of Copper (Cu) and Carbon (C) is due to the grids that were used for the analysis of the samples [20, 29] which indicates the purity of the prepared samples. The results of micrograph analysis of pristine and annealed at 950 °C titanium dioxide NP's are summarized in Table 2.

### 3.6 Monte-Carlo simulations

Monte-Carlo simulation was carried out as a representative for samples prepared using AA and AA + OM as surfactants. TiO<sub>2</sub> NP's, prepared using AA as surfactant, includes of almost spherical particles whereas the sample, prepared using AA + OM as surfactants, consists of rod-like particles. The simulation has been performed in order to understand the growth mechanism of titania in presence of various surfactants and compare with the experimental results. Hence, the simulation was performed to obtain steady state of the system and then consider the plausible interactions among the particles.

#### 3.6.1 Model description

The particles are considered as disks with diameter  $\sigma$  in this simulation and they are called as cores. The particles are surrounded by soft corona with an interaction range  $\lambda$ . In fact, in this model, the cores and coronas are considered as titania NP's and surfactants respectively. The representative of a typical core and corona is depicted in Fig. 8. Square well (SW) potential is the simplest and effective model which could mimic the structural properties of different systems like colloids, liquids, glass, and alloys. The structures can be compact or non-compact depends on the well depth and the range of interactions in the system [49–51]. In the current article, pristine and sample annealed at 950 °C are prepared using AA and AA + OM as surfactants, respectively.

These two samples are selected for simulation using Monto-Carlo model. The surfactants can modify the interactions among titania NP's. The performed simulation demonstrated a pair-wise interaction potential for the pristine sample that consists of hard-sphere repulsion and an attraction with well depth. In this case, the particles do not interact, if the distance between them is greater than interaction range ( $\lambda$ ) whereas they experience attractive interaction ( $-\epsilon_1$ ) when they are in the range of single particle diameter and interaction range ( $\lambda$ ). Additionally, the overlapping of the particles is forbidden in this system. The potential model for pristine sample is as follow (Eq. 3);

$$V(r) = \begin{cases} \infty, & r < \sigma \\ \epsilon_2, & \sigma < r < \lambda \\ 0, & r > \lambda \end{cases} \quad (3)$$

where  $\sigma$  is the diameter of the discs and  $\lambda$  is the interaction range.

As explained in the morphological section, the functional groups of carboxylic acid have been tightly bound onto the surface of titania that causes the consolidation of the individual particles and form rod-like structures for rutile titania



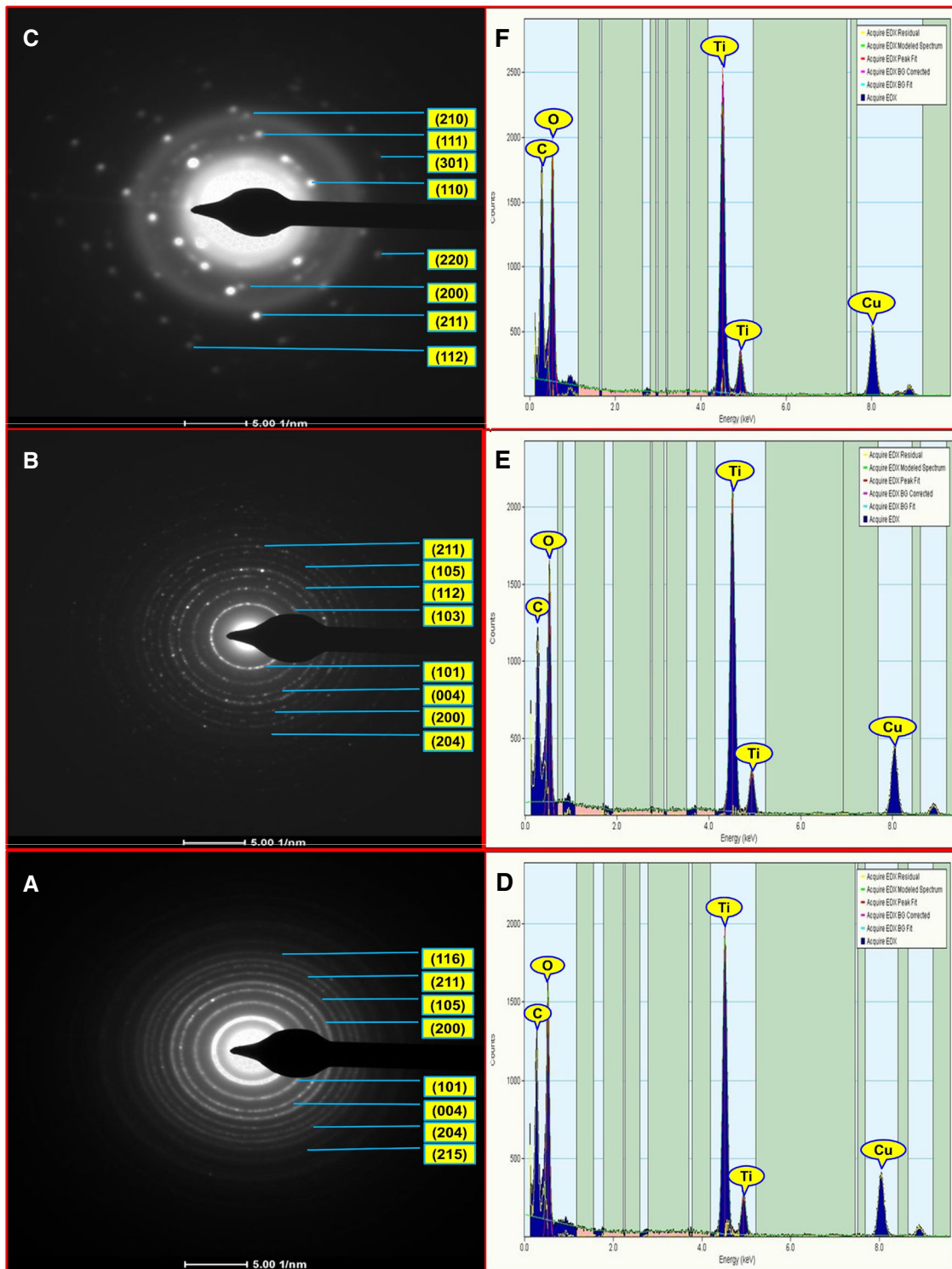


**Fig. 7** Selected area electron diffraction (SAED) and energy dispersive X-ray spectroscopy (EDS) patterns of (A, D) pristine in presence of AA, B, E and C, F calcinated at 550 and 950 °C TiO<sub>2</sub> NP's in presence of OM and AA + OM as surfactants, respectively

NP's. This might be due to repulsive interactions among titania NP's. Therefore, a repulsive step potential is introduced in simulations to explain such changes. Other development

demonstrated that system involving hard core with soft repulsive potential causes a rich phase behaviour that in turn results to solid–solid transitions [52]. The growth mechanism

**Table 2** Microscopic results obtained from TEM, SAED, and EDS of as-prepared, annealed at 950 °C titania NP’s in the existence of AA, and AA + OM as surfactants respectively

Results Tempt. (°C)	Elements	Atomic (%)	d-spacing (Å) &(hkl)	Average particle size (nm)
Pristine	Titanium	29.10	3.50	10
	Oxygen	70.89	(101)	
950 °C	Titanium	37.42	3.22	25
	Oxygen	62.57	(110)	

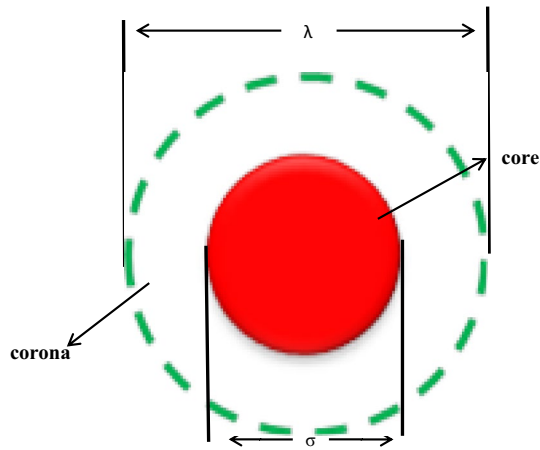


**Fig. 8** Typical representative of core (red surface or disk) and corona (dotted green). (Color figure online)

of rutile TiO<sub>2</sub> NP’s is described with the following repulsive step potential (Eq. 4);

$$V(r) = \begin{cases} \infty, & r < \sigma \\ \epsilon_2, & \sigma \leq r < \lambda \\ 0, & r \geq \lambda \end{cases} \quad (4)$$

The schematic of the potential model for pristine and rutile titania NP’s is demonstrated in Fig. 9. In this simulation, the interaction range is  $\lambda = 2.5$ ,  $\sigma$  is the unit of length,  $\epsilon_1$  and  $\epsilon_2$  are expressed in  $k_B T$  ( $K_B$  is Boltzman constant and T is the temperature). Reduced density for this system is defined as formula 5;

$$\rho^* = \rho \sigma^2 \quad (5)$$

where  $\rho = \frac{N}{A}$  is the particle density, N is number of particles, and A is the area of simulation box. The simulation was performed for moderate reduced density,  $\rho^* = 0.3$ . Reduced temperature is defined as follow (Eq. 6):

$$T^* = \frac{K_B T}{\epsilon_0} \quad (6)$$

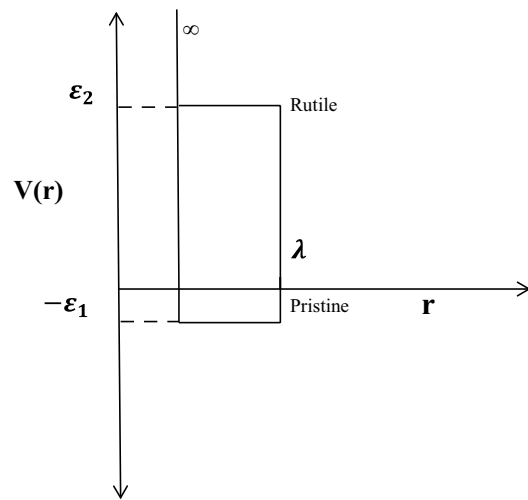


**Fig. 9** Potential well defined in the interaction model;  $\epsilon_1 = 0.5$   $\epsilon_2 = 5.0$  are for pristine and rutile titania NP’s respectively

where T is the temperature,  $k_B$  is the Boltzman constant, and  $\epsilon_0$  is the potential well depth. The number of particles was  $N = 512$  in square box with periodic boundary conditions. Monte-Carlo (MC) simulations were carried out using the canonical ensemble. The number of MC steps used for pristine and rutile titania NP’s was  $10^7$  and each step consists of approximately N particle moves.

Figure 10A depicts the simulation result for pristine TiO<sub>2</sub> NP’s with attractive square interactions. As can be seen, irregular spherical particles are randomly distributed in the system. In fact, addition of AA to the solution as a surfactant might induce the weak attraction among the particles. The estimated energy among the particles was is order of  $\approx k_B T$ . Figure 10B delineates the configuration of the system simulated for rutile titania NP’s with repulsive interactions in equilibrium condition. The particles combine to form rod-like structures when the outer layers of hard cores join together. In this alignment, the coronas of the joined particles overlap in a particular direction. This transfiguration is due to addition of OM to the solution as a surfactant that occurred at the minimum required energy.

The coronas act as spacers among rutile titania NP’s and make the periodicity in the system. Addition of OM might induce repulsive interactions among rutile titania NP’s and minimize the free energy of the system to form rod like structures. The estimated repulsive energy among rutile TiO<sub>2</sub> NP’s was about  $5 k_B T$ . The obtained results from simulation are for the system in equilibrium state. Similarly, Malessio reported the formation of such stripes/lanes with the repulsive interactions on particles with core-corona model [53].

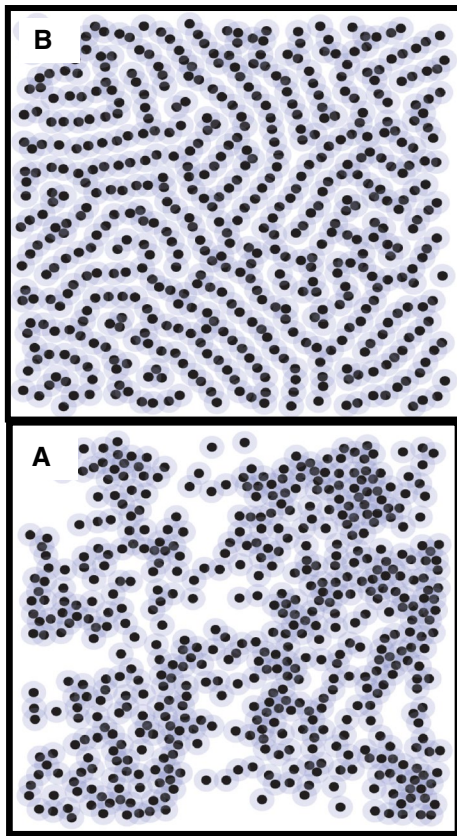


**Fig. 10** Performed simulation for **A** pristine titania NP's **B** rutile sample. The *black filled circles* represent the hard cores and the *light blue surrounds* exhibit coronas. (Color figure online)

#### 4 Conclusions and outlook

To summarize, highly crystalline and pure titania NP's have been successfully prepared using solvothermal method and the Monte-Carlo simulation was used to study the growth mechanism of  $\text{TiO}_2$  NP's. The formation of pure anatase phase in absence of annealing was proved for the as-prepared sample. The morphological study elucidated the enhancement in the particle size upon annealing and phase transformation from pure anatase to pure rutile. Interestingly, the shapes of titania NP's have been influenced by the type of surfactants and a mixture of almost disordered spherical and rounded rectangular shape were observed for the sample prepared using AA as a surfactant, whereas the shapes of sample prepared using OM as a surfactant were consisted of truncated rhombic and elongated spherical. A rod-like structure with clear grain boundaries were detected for the sample prepared using AA + OM as surfactants. Monte-Carlo simulation was performed to investigate the growth mechanism of  $\text{TiO}_2$  NP's and has suggested the predominant attractive and repulsive interactions which in turn

cause the formation of spherical and rod-like structures for as-prepared and rutile titania NP's respectively.

#### Compliance with ethical standards

**Conflict of interest** This research did not receive any specific grant from funding agencies in the public, commercial, or not-for-profit sectors.

#### References

1. L.H. Carolien, G. Albert, S. Joop, Aerosol synthesis of anatase titanium dioxide nanoparticles for hybrid solar cells. *Chem. Mater.* **15**, 4617–4624 (2003)
2. L. Hongmei, T. Tsuyoshi, L. Yungi, Zh. Jinfeng, D. Kazunari, Y. Yushan, Photocatalytic activity enhancing for titanium dioxide by co-doping with bromine and chlorine. *Chem. Mater.* **16**, 846–849 (2004)
3. D. Dastan, P.U. Londhe, N.B. Chaure, Characterization of  $\text{TiO}_2$  nanoparticles prepared using different surfactants by sol–gel method. *J. Mater. Sci.* **25**(34), 73–79 (2014)
4. D. Cao-Thang, N. Thanh-Dinh, K. Freddy, D. Trong-On, Shape-controlled synthesis of highly crystalline titania nanocrystals. *ACS Nano* **3**(11), 3737–3743 (2009)
5. D. Dastan, S. W. Gosavi, N. B. Chaure, (2015) Studies on electrical properties of hybrid polymeric gate dielectrics for field effect transistors, *Macromol. Symp.* **347**:81–86.
6. D. Dastan, A. Banpurkar, Solution processable sol–gel derived titania gate dielectric for organic field effect transistors. *J. Mater. Sci.* (2016). doi:[10.1007/s10854-016-5997-9](https://doi.org/10.1007/s10854-016-5997-9)
7. D. Dastan, N. B. Chaure, (2014) Influence of surfactants on  $\text{TiO}_2$  nanoparticles grown by Sol-Gel Technique, *J. Mater. Mech. Manufact.* **2** (1):21–24.
8. A.K. Tarek, F. Armin, R. Lars, D. Ralf, W.B. Detlef, Tailored titanium dioxide nanomaterials: anatase nanoparticles and brookite nanorods as highly active photocatalysts. *Chem. Mater.* **22**, 2050–2060 (2010)
9. S. Jakub, W. Paweł, S.-N. Magdalena, A. Halina, Raman spectroscopy of visible-light photocatalyst–nitrogen-doped titanium dioxide generated by irradiation with electron beam. *Chem. Phys. Lett.* **566**, 54–59 (2013)
10. I. Burlacov, J. Jirkovský, M. Müller, R.B. Heimann, Induction plasma-sprayed photocatalytically active titania coatings and their characterisation by micro-Raman spectroscopy. *Surf. Coat. Technol.* **201**, 255–264 (2006)
11. D. Dastan, S.L. Panahi, N.B. Chaure, Characterization of titania thin films grown by dip-coating technique. *J. Mater. Sci.* **27**, 12291–12296 (2016)
12. Ch. Anirban, K. Akira, F. Takeshi, Ch. Ming-Wei, A. Tadafumi, Nano-twinned structure and photocatalytic properties under visible light for undoped nano-titania synthesised by hydrothermal reaction in water–ethanol mixture, *J. Supercrit. Fluids* **58**:136–141. (2011)
13. M. Venu, K. G. Sanjeev, K.J. Prafulla, (2011) Low frequency Raman scattering of anatase titanium dioxide nanocrystals, *Physica E* **44**:614–617.
14. J.R. Stephanie, H. R. Al-O. Ala, L. Soo-Keun, M.S. Daniel, K.J.R. Peter, The application of Raman and anti-stokes Raman spectroscopy for in situ monitoring of structural changes in laser irradiated titanium dioxide materials. *Appl. Surf. Sci.* **252**, 7948–7952 (2006)
15. K.K. Rahul, Gh. Harshad, S. Deepa, C.Kh. Kartic, S.S. Raman, Room temperature synthesis of titanium dioxide nanoparticles of

- different phases in water in oil microemulsion. *Coll. Surf. A* **369**, 75–81 (2010)
16. Z. Nicolas, A.Z. Maria-Helena, T. Iris, H. Christof, Direct generation of titanium dioxide nanoparticles dispersion under supercritical conditions for photocatalytic active thermoplastic surfaces for microbiological inactivation, *Mater. Chem. Phys.* **153**, 274–284 (2015)
  17. Y.A. Amira, A.K. Tarek, O. Torsten, B. Detlef, Photocatalytic activities of different well-defined single crystal TiO<sub>2</sub> surfaces: anatase versus rutile. *J. Phys. Chem. Lett.* **2**, 2461–2465 (2011)
  18. Sh. Laifa, Zh. Xiaogang, L. Hongsen, Y. Changzhou, C. Guozhong, Design and tailoring of a three-dimensional TiO<sub>2</sub>-graphene-carbon nanotube nanocomposite for fast lithium storage. *J. Phys. Chem. Lett.* **2**, 3096–3101 (2011)
  19. H.Md. Nasim, M.G. Betar, J.Sh. Nisarg, Sh-H. Yang, T.H. Paula, Synthesis of highly stable sub-8 nm TiO<sub>2</sub> nanoparticles and their multilayer electrodes of TiO<sub>2</sub>/MWNT for electrochemical applications. *Nano Lett.* **13**, 4610–4619 (2013)
  20. P.S. Dipti, J. Naresh, K. Rohit, R. Sakthivel, P. Sony, T. Das, J. Kalidoss, P.S. Mukherjee, A. Tiwari, Synthesis and characterization of titania nanorods from ilmenite for photocatalytic annihilation of *E. coli*. *J. Photochem. Photobiol. B* **140**, 69–78 (2014)
  21. W. Zubin, T. Qunwei, H. Benlin, Ch. Xiaoxu, Ch. Haiyan, L. Yu, Titanium dioxide/calcium fluoride nanocrystallite for efficient dye sensitized solar cell. A strategy of enhancing light harvest. *J. Power Sour.* **275**, 175–180 (2015)
  22. G. Hanyang, H. Guoxin, Sh. Wenfeng, Zh. Kunxu, (2014) Colloidal monolayer titania quantum dots prepared by hydrothermal synthesis in supercritical water, *J. Supercrit. Fluids* **88**:126–133.
  23. A.V. Anuj, M. Krishnamurthi, Effect of anatase-brookite mixed phase titanium dioxide nanoparticles on the high temperature decomposition kinetics of ammonium perchlorate, *Mater. Chem. Phys.* **139**, 537–542 (2013)
  24. Zh. Guo-Wen, H. Guo-Hua, X. Wei-Liang, X. Xiong-Fa, L. Dan-Ni, Y.-H. Xu, Enhanced photocatalytic performance of titania nanotubes modified with sulfuric acid. *J. Mol. Catal. A* **363**(364), 423–429 (2012)
  25. R. Jiang, H.-Y. Zhu, H.-H. Chen, J. Yao, Y.-Q. Fu, Z.-Y. Zhang, Y.-M. Xu, Effect of calcination temperature on physical parameters and photocatalytic activity of mesoporous titania spheres using chitosan/poly(vinyl alcohol) hydrogel beads as a template. *Appl. Surf. Sci.* **319**, 189–196 (2014)
  26. M.F. Vanesa, L.S. Edgardo, N.B. Mirta, R.P. Luis, Direct modification with tungstophosphoric acid of mesoporous titania synthesized by urea-templated sol-gel reactions. *J. Coll. Interface Sci.* **327**, 403–411 (2008)
  27. N.Sh. Godlisten, S.M. Imran, J.J. Sun, E. Marion, A. Nadir, M.S. Haider, S.J. Kang, H.T. Kim, Sol-gel synthesis of photoactive zirconia-titania from metal salts and investigation of their photocatalytic properties in the photodegradation of methylene blue. *Powder Technol.* **258**, 99–109 (2014)
  28. Ch. Wei-Lun, S. Hung-Wei, Ch. Wen-Chang, Synthesis and properties of photosensitive polyimide-nanocrystalline titania optical thin films. *Eur. Polym. J.* **45**, 2749–2759 (2009)
  29. A.E. Shalan, M.M. Rashad, Y. Youhai, L.-C. Monica, M.S.A. Abdel-Mottaleb, Controlling the microstructure and properties of titania nanopowders for high efficiency dye sensitized solar cells. *Electrochim. Acta* **89**, 469–478 (2013)
  30. N.Sh. Godlisten, E. Marion, S.M. Imran, J.J. Sun, T.K. Hee, Sol-gel synthesis of photoactive kaolinite-titania: effect of the preparation method and their photocatalytic properties. *Appl. Surf. Sci.* **331**, 98–107 (2015)
  31. B. Muhammad-Sadeeq, L. Cheng, Z. Yinxiang, Y. Minghao, W. Qili, M. Wu, Z. Lu, Y. Tong, Titanium dioxide@titanium nitride nanowires on carbon cloth with remarkable rate capability for flexible lithium-ion batteries. *J. Power Sour.* **272**, 946–953 (2014)
  32. N.Sh. Godlisten, E. Gideon, V.Q. Dang, N.K. You, H.Sh. Young, A. Hilonga, J.-K. Kim, H.T. Kim, Two step synthesis of a mesoporous titania-silica composite from titanium oxychloride and sodium Silicate. *Powder Technol.* **217**, 489–496 (2012)
  33. Y. J. Kyeong, B. P. Seung, A. Masakazu, (2005) Photoluminescence and photoactivity of titania particles prepared by the sol-gel technique: effect of calcination temperature, *J. Photochem. Photobiol. A* **170**:247–252.
  34. N.R. Khalid, E. Ahmed, H. Zhanglian, M. Ahmad, Synthesis and photocatalytic properties of visible light responsive La/TiO<sub>2</sub>-graphene composites. *Appl. Surf. Sci.* **263**, 254–259 (2012)
  35. A. Bahari, A. Qhavami, Electrical and nanostructural characteristics of R-, Fe-, S-CNT electrodes of microbial field effect transistors. *J. Mater. Sci.* **27**, 5934–5942 (2016)
  36. R. Gholipur, A. Bahari, DNG Metamaterials: preparation and characterization of silver nanoparticles in the dielectric medium. *Mater. Lett.* **180**, 123–126 (2016)
  37. M. Shahbazi, A. Bahari, Sh. Ghasemi, Studying saturation mobility, threshold voltage, and stability of PMMA-SiO<sub>2</sub>-TMSPM nano-hybrid as OFET gate dielectric. *Synth. Met.* **221**, 332–339 (2016)
  38. C.Y. Jimmy, Y. Jiaguo, H. Wingkei, J. Zitao, Zh. Lizhi, Effects of F-doping on the photocatalytic activity and microstructures of nanocrystalline TiO<sub>2</sub> powders. *Chem. Mater.* **14**, 3808–3816 (2002)
  39. F.M. Hasmath, M. Sankaran, Photo-decolorization and detoxification of toxic dyes using titanium dioxide impregnated chitosan beads. *Int. J. Biol. Macromol.* **70**, 420–426 (2014)
  40. Y. Yongheng, X. Tao, H. Guangwei, J. Zhongyi, W. Hong, Fabrication of sulfonated poly(ether ether ketone)-based hybrid proton-conducting membranes containing carboxyl or aminoacid-functionalized titania by in situ sol-gel process. *J. Power Sour.* **276**, 271–278 (2015)
  41. X. Tao, H. Weiqiang, Sh. Xiaohui, W. Hong, L. Xicheng, J. Wang, Zh. Jiang, Sulfonated titania submicrospheres-doped sulfonated poly(ether ether ketone) hybrid membranes with enhanced proton conductivity and reduced methanol permeability. *J. Power Sour.* **196**, 4934–4942 (2011)
  42. L. P. Donald, M. L. Gary, S. K. George, *Introduction to spectroscopy*, 3rd edn. (Thomson Learning, Washington DC, 2001), pp. 20–100.
  43. D. Archana, K.S. Brijesh, D. Joydeep, P.K. Dutta, In vivo evaluation of chitosan-PVP-titanium dioxide nanocomposite as wound dressing material. *Carbohydr. Polym.* **95**, 530–539 (2013)
  44. K. E. Saisy, K. K. Suma, J. Rani, (2012) Effect of titanium dioxide on the thermal ageing of polypropylene, *Polym. Degrad. Stab.* **97**:615–620.
  45. S. Aihua, L. Zhixiang, L. Ming, X. Gaojie, L. Yong, P. Cui, Room temperature synthesis of spherical mesoporous titania. *Powder Technol.* **201**, 130–137 (2010)
  46. L. H. Rohan, A. C. Jonathan, L. Rasmus, M. H. James, P. B. Robert, (2011) In-situ preparation of poly(2-hydroxyethyl methacrylate)-titania hybrids using G-radiation, *Polymer*, **52**:4471–4479.
  47. V. Iswarya, M. Bhuvaneshwari, A.A. Sruthi, I. Siddharth, Ch. Gouri, P.T. Chandrasekaran, G.M. Bhalerao, S. Chakravarty, A.M. Raichur, N. Chandrasekaran, A. Mukherjee, Combined toxicity of two crystalline phases (anatase and rutile) of titania nanoparticles towards freshwater microalgae: *chlorella* sp. *Aquat. Toxicol.* **161**, 154–169 (2015)
  48. W. Ming, L. Yanqiong, Zh. Junmin, G. Weimin, L. Yuncang, C. Wen, P. Hodgson, Synthesis and characterization of nanostructured Ag on porous titania. *Appl. Surf. Sci.* **257**, 4836–4843 (2011)

49. P.S. Mohanty, D. Paloli, J.J. Crassous, E. Zaccarelli, P. Schurtenberger, Effective interactions between soft-repulsive colloids: experiments, theory, and simulations. *J. Chem. Phys.* **140**, 0949011–09490110 (2014)
50. G. Malescio, Complex phase behavior from simple potentials. *J. Phys.* **19**, 0731011–07310123 (2007)
51. J.B. Delfau, H. Ollivier, C. Lopez, B. Blasius, E. Emilio Hernandez Gar C, Pattern formation with repulsive soft-core interactions: discrete particle dynamics and Dean-Kawasaki equation. *Phys. Rev. E* **94**, 0421201–04212013 (2016)
52. J. Fornleitner, G. Kahl, (2008) Lane formation Vs. cluster formation in two-dimensional square-shoulder systems—a genetic algorithm approach *EPL*, 82:180011–180016.
53. G. Malescio, G. Pellicane, Stripe patterns in two-dimensional systems with core-corona molecular architecture. *Phys. Rev. E* **70**, 0212021–0212026 (2005)